3.1 LOW ACTIVATION JOINING OF SiC/SiC COMPOSITES FOR FUSION APPLICATIONS: THERMOMECHANICAL MODELING OF DUAL-PHASE MICROSTRUCTURES AND DISSIMILAR MATERIAL JOINTS—B.N. Nguyen, C.H. Henager, Jr., and R.J. Kurtz; (Pacific Northwest National Laboratory, Richland, WA, USA); M. Ferraris, (Politecnico di Torino, Torino, Italy); Y. Katoh, (Oak Ridge National Laboratory, Oak Ridge, TN, USA)

OBJECTIVE

Finite element (FE) continuum damage mechanics (CDM) models have been developed to simulate and model dual-phase joints and cracked joints for improved analysis of SiC materials in nuclear environments. This report extends the analysis from the last reporting cycle by including preliminary thermomechanical analyses of cracked joints and implementation of dual-phase damage models.

SUMMARY

Miniature torsion specimens were designed for joint testing and irradiation in test reactors with limited irradiation volumes since SiC and SiC-composites used in fusion environments are thought to require joining methods for component assembly. HFIR irradiation results indicated two broad types of joint damage due to irradiation at either 500˚C or 800˚C to 3 dpa or 5 dpa. One type of damage can be categorized as microcracking within multi-phase joints at the micron length scale. The other type of damage can be categorized as cracking within the miniature torsion sample and within the joint where the cracks are now on the scale of the joint thickness and are not considered to be microcracks. This report expands the methods developed and discussed in our previous report to model both types of cracking due to thermal stresses caused by the mismatch of thermoelastic properties (i.e., elastic properties and thermal expansion coefficients) in the constituent phases or between the joint and joint materials for a specimen uniformly heated from 28˚C to 800˚C.

PROGRESS AND STATUS

Introduction

The international fusion materials community has irradiated and is currently irradiating several joint types and compositions in the HFIR reactor at ORNL [1]. PNNL is working with Politecnico di Torino (POLITO) and ORNL using miniature torsion specimens that have been specifically designed for pre- and post-irradiation joint shear strength testing [2]. To elucidate how cracks initiate and propagate in the torsion joint specimens, FE analyses of these specimens subjected to torsion were previously performed using a CDM model developed at PNNL for elastic and elastic-plastic materials for which any nonlinearity in stress/strain response is due solely to damage and not to other irreversible processes such as plasticity [3-5]. The CDM model was implemented in the ABAQUS® finite element code via user subroutines. This CDM model [3] was also applied at the submicron scale where the OOF2[1] software package was used to create a dual-phase mesh within the joint region from an optical micrograph of a joint. The constitutive behavior of each phase in the modeling domain was described by the CDM model. Our study was conducted to explore the effects of differential material responses within the joint to external forces, such as thermal expansion, swelling, and applied loads. Although the joints survived the HFIR irradiation with reasonable properties, there was degradation observed in scanning electron microscope (SEM) images taken post-irradiation at ORNL. This report expands the methods developed and discussed in our previous reports to understand the sources for the observed cracking and subsequent joint degradation due to uniform temperature changes so that improved joints can be fabricated for fusion applications.

Model Formulation

Approach

This section provides a summary of the damage model implemented in ABAQUS® via user subroutines for the analyses of the joint specimen and of the dual-phase Ti_3SiC_2/SiC microstructural model [3-5]. The constitutive relations of the elastic damage model accounting for thermal stresses are given by:

[1] NIST software, see http://www.ctcms.nist.gov/oof/oof2/

$$\sigma_{ij} = C_{ijkl}(T,D)(\varepsilon_{ij} - \varepsilon_{ij}^{\mathrm{th}}) = C_{ijkl}^{0}(T)(1-D)(\varepsilon_{ij} - \varepsilon_{ij}^{\mathrm{th}}) = C_{ijkl}^{0}(T)(1-D)\varepsilon_{ij}^{\mathrm{m}} \tag{1}$$

where $C_{ijkl}(T,D)$ is the material elastic stiffness tensor that varies with temperature T and is affected by the microcracking damage phenomenologically described by the damage variable, D. In Eq. (1), decoupling between the damage and thermal effects is assumed, and the elastic stiffness tensor is assumed to vary linearly with D. ε_{ij}, $\varepsilon_{ij}^{\mathrm{th}}$ and $\varepsilon_{ij}^{\mathrm{m}}$ are the total, mechanical and thermal strains, respectively. $\varepsilon_{ij}^{\mathrm{th}}$ is computed from the coefficients of thermal expansion (CTEs) $\alpha_{ij}(T)$ and temperature change ΔT as

$$\varepsilon_{ij}^{\mathrm{th}} = \alpha_{ij}(T)\Delta T \tag{2}$$

The damage evolution law was obtained from concepts of thermodynamics of continuous media [6, 7] and a damage criterion dependent on the damage threshold function $F_{\mathrm{c}}(T,D)$ can be expressed as:

$$\mathrm{d}D = \frac{\dfrac{\partial C_{ijkl}(T,D)}{\partial D}\varepsilon_{ij}^{\mathrm{m}}\,\mathrm{d}\varepsilon_{kl}^{\mathrm{m}}}{\dfrac{\partial F_{\mathrm{c}}(T,D)}{\partial \mathrm{D}}} \tag{3}$$

This damage evolution law can describe microcracking damage caused by tensile stresses [3] or shear damage caused by shear stresses [5]. As ceramics may not suffer from microcracking under a compressive stress state, at this stage of the model development, damage is not activated under a compressive state of stress.

Identification of Temperature-dependent Thermomechanical properties

The integration of the constitutive relation requires identification of the thermomechanical properties including the damage threshold function as functions of temperature for the temperature range of interest. Measured temperature-dependent elastic modulus data from [8] and [9] were used for SiC and Ti_3SiC_2, respectively. The measured temperature-dependent thermal expansion data from [8] were used for SiC and from [10, 11] for Ti_3SiC_2. For the joint, homogenized thermoelastic properties of Ti_3SiC_2/SiC are needed for treating the joint as a continuum at the macroscopic scale. Thus, an Eshelby-Mori-Tanaka approach (EMTA) [12] was used to compute the elastic modulus and CTEs of Ti_3SiC_2/SiC using the constituent data and considering 50% volume fraction for each phase and uniform distribution of Ti_3SiC_2 in SiC. The temperature dependence of these properties is given in Figure 1.

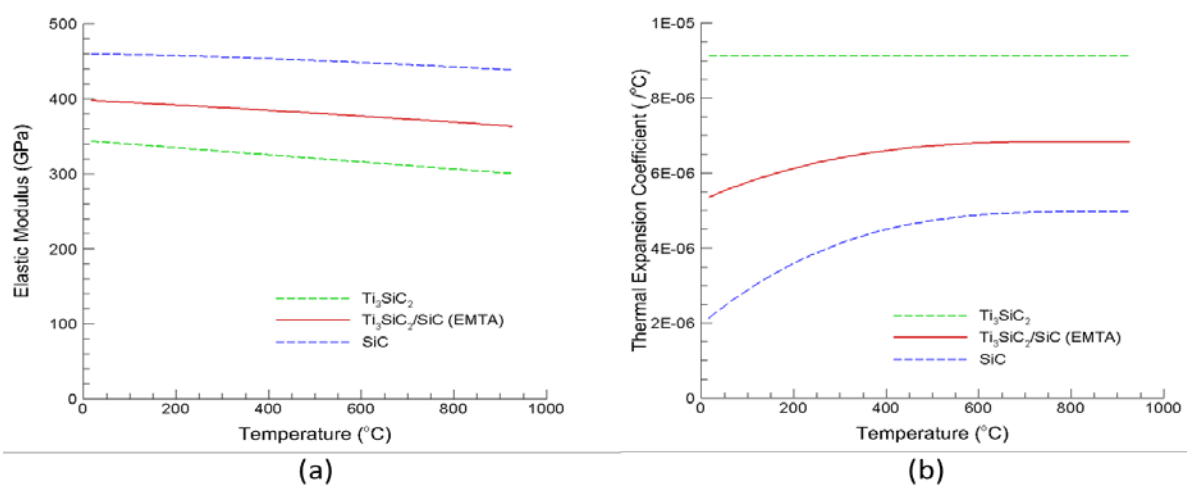

Figure 1. (a) Temperature-dependent elastic modulus and (b) CTEs for Ti_3SiC_2, Ti_3SiC_2/SiC composite (EMTA prediction), and SiC from the literature [8-11].

Results

Analysis of the Joint Specimen Subjected to Uniform Temperature Increase

The joint specimen subjected to torsion analyzed in [5] and also discussed in our previous report [13] has been further analyzed during this reporting period for thermal stresses and their effect on joint integrity. To this end an unconstrained joint specimen was subjected to a uniform temperature increase from room temperature to 800˚C, which was the temperature at which the specimen underwent neutron irradiation in HFIR. Figure 2 shows the FE mesh of the joint specimen with the associated material assignments from [5]. The thermoelastic properties presented in Figure 1 were assigned to the respective materials of the joint specimen structure for the ABAQUS® analysis using the damage model.

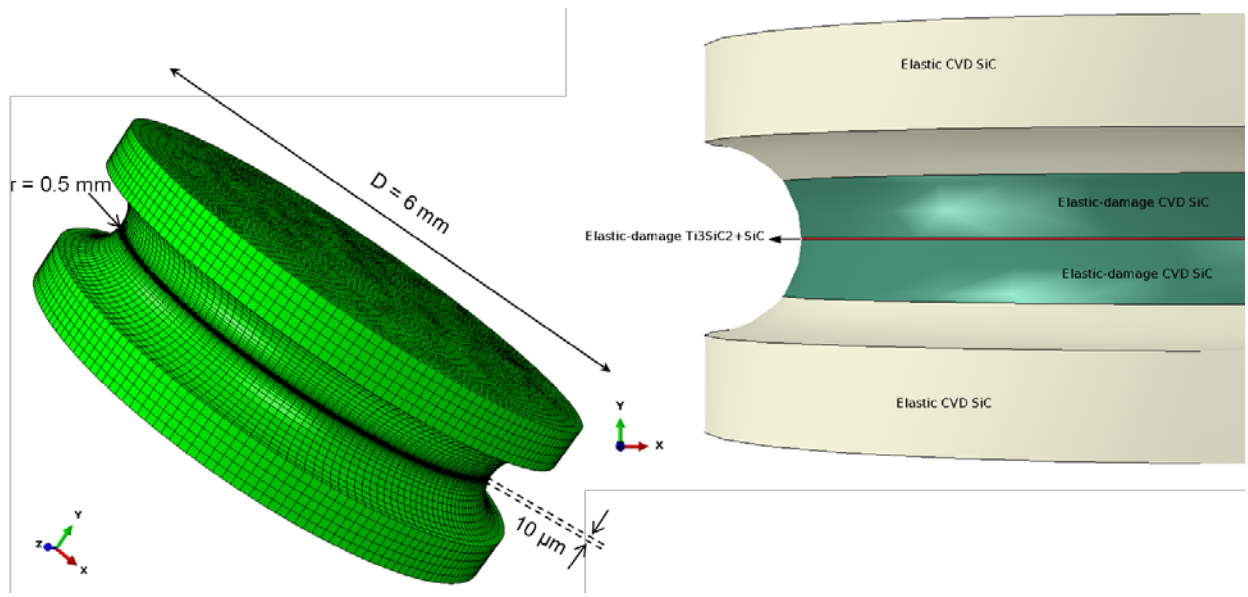

Figure 2. A FE mesh with the associated material assignments studied in [5].

Figure 3 respectively shows the uniform temperature distribution (Figure 3a) at 800˚C in the specimen, the contours of the most important stress components, σ_{rr} (Figure 3b) and σ_{tt}(Figure 3c) as well as the damage distribution in the specimen (Figure 3d) through a zoomed-in section showing the notch and the joint. Brought to 800˚C, the specimen experienced high compressive stresses in the joint but tensile stresses in the adjacent CVD-SiC region at the notch. This stress state resulted from the mismatch of CTEs between SiC and Ti_3SiC_2/SiC (Figure 1b). The CTEs of SiC are significantly lower than the values for the Ti_3SiC_2/SiC joint for the whole temperature range. The thermal expansion of the Ti_3SiC_2/SiC joint was constrained by the lesser expansion of SiC. Stress concentrations caused minor damage at the notch in the CVD-SiC along the joint/SiC interface. The damage distribution at 800˚C, presented in Figure 3c, shows very little damage at the notch. The damage variable value attained in this area was about 0.06, which was very low compared to the value at damage saturation (= 0.2). Small but confined damage at the notch and along the joint/SiC interface is evidence for the existence of some interface cracks prior to irradiation that could grow during irradiation under the right conditions. Low tensile stresses are also observed in the other areas of SiC away from the joint.

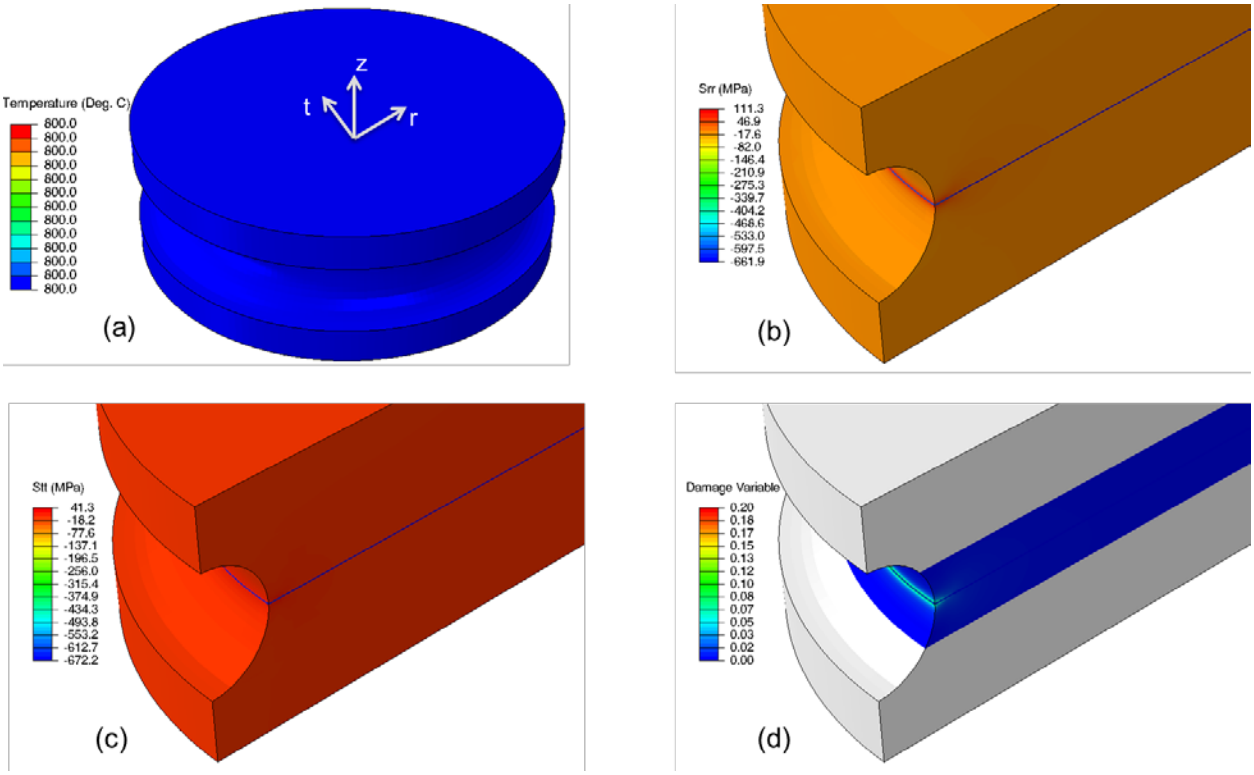

Figure 3. (a) The joint specimen uniformly brought to 800°C, (b) contour of the radial stress, σ_{rr}, (c) contour of the tangential stress, σ_{tt}, and (d) damage distribution at 800°C.

Analysis of the Ti_3SiC_2/SiC Dual Phase Microstructural Model

As discussed in Reference [1] and in our previous semiannual report [13], miniature torsion joints were irradiated in HFIR at ORNL and examined post-irradiation using SEM. Archival joints were imaged and tested pre-irradiation for comparison. Joint images showed two types of damage that is assumed to have originated from the neutron irradiation in HFIR for several of the joints. However, in view of the significant mismatches of thermoelastic properties between SiC and Ti_3SiC_2, and between SiC and the Ti_3SiC_2/SiC composite, thermal stresses caused by large temperature changes could contribute to microcracking of the joint prior to irradiation. This is the subject of our current investigation. One type of damage can be categorized as microcracking within multi-phase joints at the micron and sub-micron length scale. The other type of damage discussed in the previous section can be categorized as cracking within the miniature torsion sample and within the joint where the cracks are on the scale of the joint thickness. The present section addresses microcracking at the microstructural level.

In our previous report, a FE mesh of the joint microstructure using the OOF2 public domain software was presented. A digital image that was 14.1 µm on a side (910 x 910 pixels) was input to OOF2 and used to create a dual-phase FE mesh consisting of 230,000 nodes, containing both triangular and quadrilateral elements. This allowed a detailed discretization of the microstructure at the phase boundaries and the ability for ABAQUS® to assign individual constitutive laws to each phase. The meshed microstructure and constituent phase distribution presented in our previous report [13] are shown in Figure 4. In this report, the same microstructural model subjected to uniform temperature increase was analyzed by ABAQUS® using the damage model in order to investigate the thermal stresses that could cause microcracking.

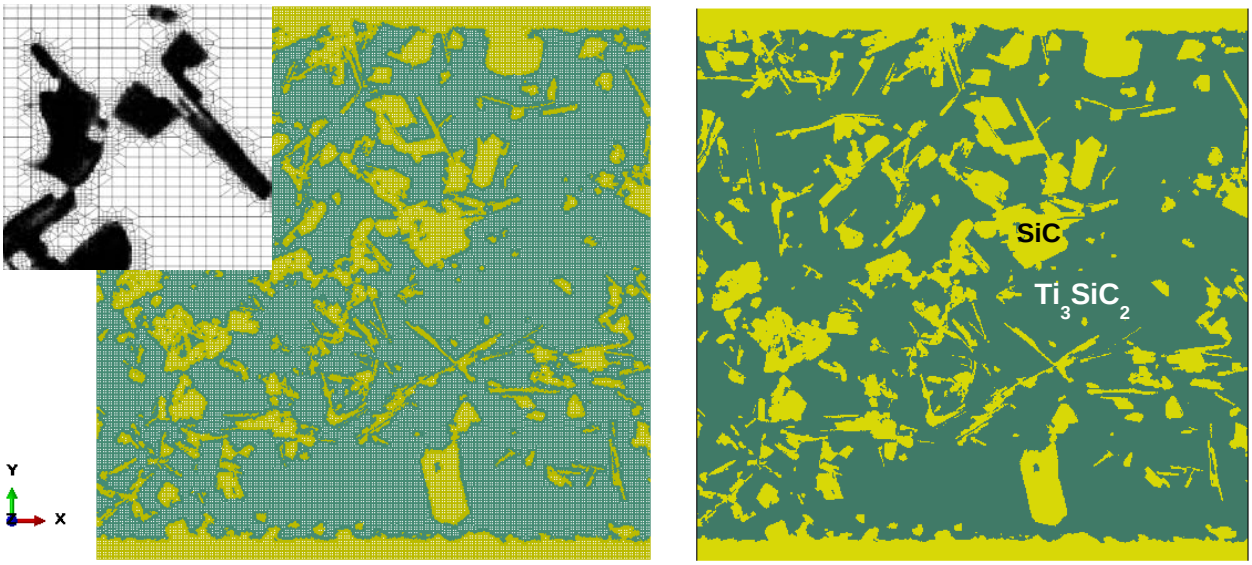

Figure 4. (a) The FE mesh is superimposed on the image of the microstructure. The insert in (a) shows the high-resolution mesh at the interfaces between the SiC (black) and the ternary MAX Ti_3SiC_2 (white) phase and (b) the same image with the two phases identified within the joint.

Figure 5 shows the uniform temperature distribution (Figure 5a) about 200°C in the specimen, the damage distribution (Figure 5b), and the contours of the principal stress components, σ_{xx} (Figure 5c) and σ_{yy} (Figure 5d). Referring to Figure 4 for the phase distribution, Figure 5b shows significant development of damage in the SiC phase. Many microcracks occurred in the SiC elements where the damage variable reached the saturation value (0.2). Microcracking of the SiC phase along the SiC/dual-phase joint interface is also observed in Figure 5b. The contours of stress distributions given in Figure 5c and Figure 5d reveal relatively high tensile stresses in all the SiC elements. The lower SiC phase region along the interface with the joint experienced high tensile stresses, σ_{xx}. Locally high tensile stresses in some SiC elements have caused failure of these elements observed in Figure 5b. The important mismatches between the thermoelastic properties of SiC and Ti_3SiC_2, in particular, the CTE mismatch were in part responsible for the stress state observed in Figure 5. There might be other mechanisms that would reduce the stresses in the SiC elements in the microstructure that will need to be investigated and potentially included in the model.

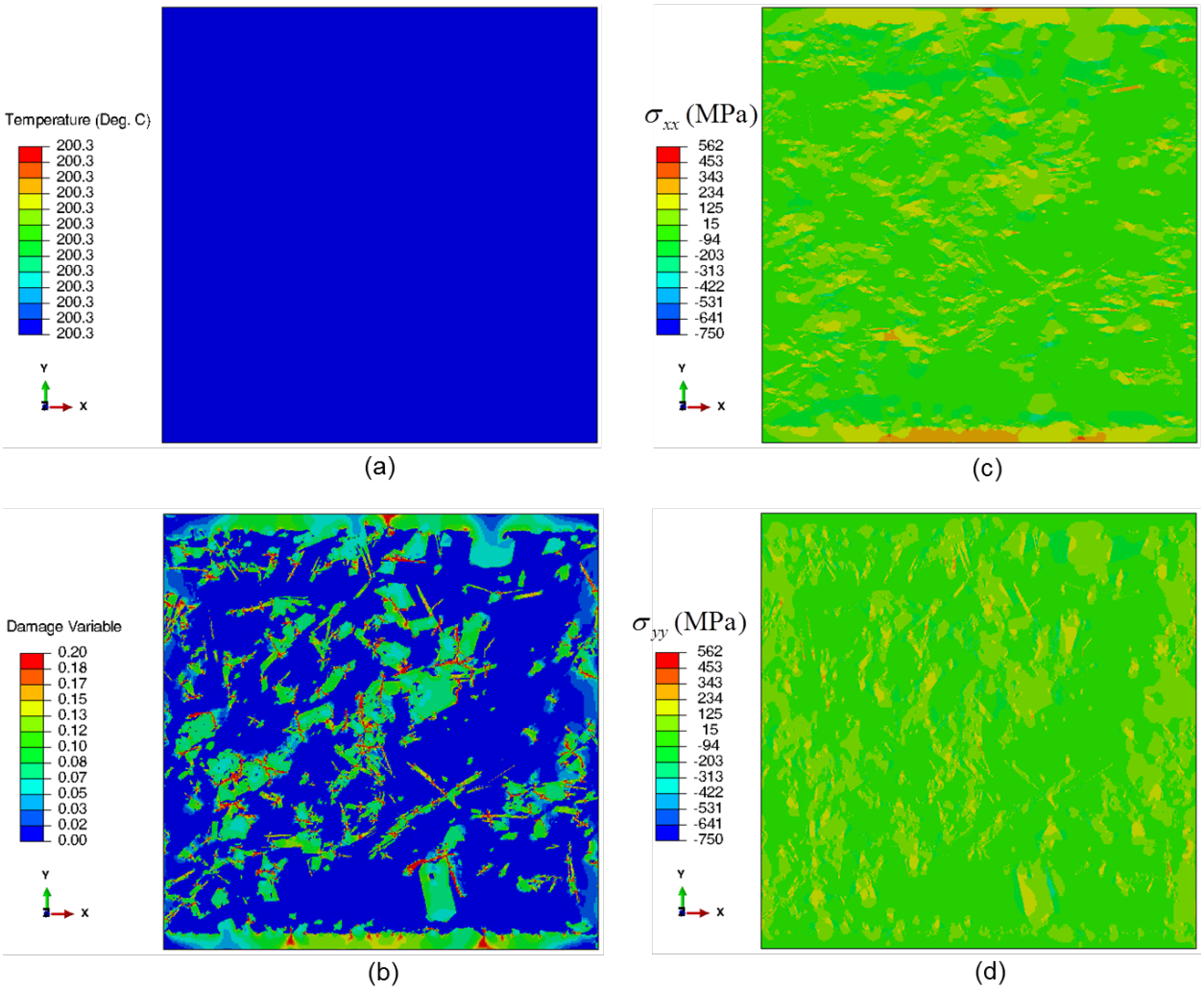

Figure 5. (a) Temperature reached 200.3°C during temperature increase application, (b) contour of the damage variable, (c) stress component, σ_{xx}, and (d) stress component, σ_{yy} at T=200.3°C.

Conclusion

A modification of the PNNL CDM model [4, 5] implemented in ABAQUS® to include thermal loading has been shown to provide qualitative agreement with experimental observations following SiC joint irradiations in HFIR. Both in-plane and transverse cracks are simulated and the overall damage distributions predicted appear to be in agreement with limited SEM observations of irradiated joints that indicated microcracks nucleating within the dual-phase joint region at SiC/Ti_3SiC_2 interface boundaries. At this stage, we have focused on the thermal stresses as this effect may cause microcracking in the joint or at the interface boundaries prior to irradiation solely due to temperature increases in HFIR.

Future Work

The developed FE CDM model will be modified to account for thermophysical and swelling loads consistent with the HFIR irradiation conditions.

Acknowledgements

This research was supported by Office of Fusion Energy Sciences, U.S. Department of Energy (DOE) under Contract DE-AC05-76RL01830.

References

[1] Katoh, Y., L.L. Snead, T. Cheng, C. Shih, W.D. Lewis, T. Koyanagi, T. Hinoki, C.H. Henager Jr, and M. Ferraris, J. Nucl. Mater., 2014. 448(1-3): p. 497-511.
[2] Jung, H.-C., T. Hinoki, Y. Katoh, and A. Kohyama, J. Nucl. Mater., 2011. 417(1-3): p. 383-386.
[3] Nguyen, B.N., B.J. Koeppel, S. Ahzi, M.A. Khaleel, and P. Singh, J. Am. Ceram. Soc., 2006. 89(4): p. 1358-1368.
[4] C. H. Henager, J., B.N. Nguyen, R.J. Kurtz, M. Ferraris, and Y. Katoh, in *Fusion Reactor Materials Program Semiannual Progress Reports*, Vol. 58, F. Wiffen, R. Godfrey, and B. Waddell, Editors. 2015, ORNL: Oak Ridge, TN. p. 108-118
[5] Henager, C.H., B.N. Nguyen, R.J. Kurtz, T.J. Roosendaal, B.A. Borlaug, M. Ferraris, A. Ventrella, and Y. Katoh, J. Nucl. Mater., 2015. 466: p. 253-268.
[6] Maugin, G.A., *The Thermomechanics of Plasticity and Fracture*. 1992, Cambridge, UK: Cambridge University Press.
[7] Lemaitre, J. and J.L. Chaboche, Journal de Mecanique Appliquee, 1978. 2(3): p. 317-65.
[8] Snead, L.L., T. Nozawa, Y. Katoh, B. Thak-Sang, S. Kondo, and D.A. Petti, J. Nucl. Mater., 2007. 371(1-3): p. 329-77.
[9] Barsoum, M.W., M. Radovic, A. Ganguly, T. Zhen, P. Finkel, S.R. Kalidindi, and E. Lara-Curzio, Acta Mater., 2006. 54(10): p. 2757-67.
[10] Manoun, B., S.K. Saxena, H.P. Liermann, and M.W. Barsoum, J. Am. Ceram. Soc., 2005. 88(12): p. 3489-91.
[11] Barsoum, M.W., T. El-Raghy, C.J. Rawn, W.D. Porter, H. Wang, E.A. Payzant, and C.R. Hubbard, Journal of the Physics and Chemistry of Solids, 1999. 60(4): p. 429-39.
[12] Nguyen, B.N., *EMTA User's Guide*. 2010, Pacific Northwest National Laboratory: Richland, WA.
[13] C. H. Henager, J., B.N. Nguyen, R.J. Kurtz, M. Ferraris, and Y. Katoh, in *Fusion Reactor Materials Program Semiannual Progress Reports*, Vol. 59, F. Wiffen, R. Godfrey, and B. Waddell, Editors. 2015, ORNL: Oak Ridge, TN. p. 72-78